Magnetic Structures of Orthorhombic Li2M(SO4)2 (M = Co, Fe) and LixFe(SO4)2 (x = 1, 1.5) Phases

Laura Lander, Marine Reynaud, Juan Rodríguez-Carvajal, Jean-marie Tarascon, Gwenaëlle Rousse

Magnetic structures of orthorhombic $Li_2M(SO_4)_2$ (M = Co, Fe) and $Li_xFe(SO_4)_2$ (x = 1, 1.5) phases

Laura Lander[a,b,c], Marine Reynaud[d], Juan Rodríguez-Carvajal[e], Jean-Marie Tarascon[a,b,c] and Gwenaëlle Rousse[a,b,c,*]

[a] UMR8260 "Chimie du Solide et Energie", Collège de France, 11 place Marcelin Berthelot, 75231 Paris Cedex 05, France

[b] Réseau sur le Stockage Electrochimique de l'Energie (RS2E), FR CNRS 3459, France

[c] Sorbonne Universités – UPMC Univ Paris 06, 4 Place Jussieu, 75005 Paris, France

[d] CIC Energigune, Albert Einstein 48, 01510 Miñano (Vitoria, Álava), Spain

[e] Institut Laue-Langevin (ILL), BP 156, 6 rue Jules Horowitz, 38042 Grenoble cedex 9, France

* Corresponding author: gwenaelle.rousse@college-de-france.fr

Keywords

magnetism, Li-ion batteries, sulfates, neutron powder diffraction, magnetic structure, super-super-exchange interactions, magneto-electric effect

Abstract

We report herein on the magnetic properties and structures of orthorhombic $Li_2M(SO_4)_2$ (M = Co, Fe) and their oxidized phases $Li_xFe(SO_4)_2$ (x = 1, 1.5), which were previously studied as potential cathode materials for Li-ion batteries. The particular structure of these orthorhombic compounds (space group *Pbca*) consists of a 3D network of isolated MO_6 octahedra enabling solely super-super-exchange interactions between transition metals. We studied the magnetic properties of these phases via temperature-dependent susceptibility measurements and applied neutron powder diffraction experiments to solve their magnetic structures. All compounds present an antiferromagnetic long-range ordering of the magnetic spins below their Néel temperature. Their magnetic structures are collinear and follow a spin sequence (+ + – – – – + +), with the time reversal associated with the inversion center, a characteristic necessary for a linear magneto-electric effect. We found that the orientation of the magnetic moments varies with the nature of M. While $Li_2Co(SO_4)_2$ and $Li_1Fe(SO_4)_2$ adopt the magnetic space group *Pb'c'a'*, the magnetic space group for $Li_2Fe(SO_4)_2$ and $Li_{1.5}Fe(SO_4)_2$ is $P112_1'/a$ which might hint for a possible monoclinic distortion of their nuclear structure. Moreover we compared the orthorhombic phases to their monoclinic counterparts as well as to the isostructural orthorhombic $Li_2Ni(SO_4)_2$ compound. Finally, we show that this possible magneto-electric feature is driven by the topology of the magnetic interactions.

Introduction

Through the years, research on Li-ion batteries has produced multitude of novel materials which perform poorly as electrode materials but show a panoply of exciting physical properties such as superconductivity in $Na_xCoO_2.nH_2O$[1,2] (derived from the profoundly studied $LiCoO_2$), or multiferroic properties in $LiCoPO_4$ and $LiNiPO_4$.[3] Similarly, $LiFeAs_2O_7$, which was initially studied for its Li extraction capability[4] but soon disregarded because of the presence of As, presents an incommensurate cycloidal structure below 35 K.[5] The reverse is also true as witnessed by the recently attractive electrochemical properties of Li_2MO_3 (M=Ru, Ir) phases, which have been long explored for their thermoelectric and magnetic properties.[6,7]

Such an apparent link between magnetic and electrochemical properties in a defined compound is not fortuitous but simply rooted in the fact that both the electrochemical potential of the redox couple as well as the magnetic interactions are governed by the iono-covalency of the metal-oxygen bond. Along that line our group had previously tried to establish a correlation between T_N and the Fe^{3+}/Fe^{2+}redox potential in Fe-based polyanionic compounds[8] such as borates, phosphates and fluorosulfates.[9–15] Expanding the knowledge of the magnetism-electrochemistry interplay might help to develop technologically interesting devices not only for the battery community but also for other research fields such as multiferroics.

We recently described a new family of bisulfates $Li_2M(SO_4)_2$ (M = Mn, Fe, Co, Ni, Zn, Mg), which crystallize in two polymorphic configurations – monoclinic and orthorhombic.[16,17] Thanks to the inductive effect, the two $Li_2Fe(SO_4)_2$ polymorphs exhibit redox potentials above 3.8 V *vs.* Li^+/Li^0 upon electrochemical cycling.[8] The isolated MO_6 octahedra in the structural framework of both polymorphs solely allow M-O-O-M super-super-exchange interactions between the metal centers, which turns them into interesting model compounds for magnetic studies. Indeed, monoclinic $Li_2M(SO_4)_2$ (M = Fe, Co) and orthorhombic $Li_2Ni(SO_4)_2$ presented a long-range antiferromagnetic ordering with a possible magnetoelectric effect for the latter.[18,19]

The particular magnetic properties of orthorhombic $Li_2Ni(SO_4)_2$, where time reversal is associated to the inversion center, motivated us to examine also the isostructural orthorhombic phases $Li_2Fe(SO_4)_2$ and $Li_2Co(SO_4)_2$ and to expand the magnetic studies to other 3d transition

metals in these orthorhombic bisulfates. In particular, we aim to know if the time reversal in $Li_2Ni(SO_4)_2$ is specific to Ni^{2+} or rather to the orthorhombic structure and the topology of super-super-exchange pathways. In other words, the purpose of this study is to examine if any other transition metal, besides Ni^{2+}, pertaining to the orthorhombic $Li_2M(SO_4)_2$ structure would also order magnetically with time reversal associated with inversion. To answer this question we herein report a detailed study of the temperature-dependent magnetic susceptibility of orthorhombic $Li_2Co(SO_4)_2$ and $Li_xFe(SO_4)_2$ (x = 1, 1.5, 2). We further use powder diffraction to determine their ground-state magnetic structures and we show that the whole series of compounds would potentially present a magneto-electric effect.

Experimental section

Samples preparation

The samples of orthorhombic $Li_2M(SO_4)_2$ (*M* = Co, Fe) were prepared by mechanical milling following a previously reported procedure.[17] $Li_2Co(SO_4)_2$ was obtained after ball-milling stoichiometric amounts of anhydrous $CoSO_4$ and Li_2SO_4 for 10 hours under air using a Retsch PM100 planetary mill, whereas $Li_2Fe(SO_4)_2$ was obtained from a mixture of anhydrous $FeSO_4$ and Li_2SO_4 ground for 10 hours under argon atmosphere in order to avoid the oxidation of Fe^{+II} into Fe^{+III}.

In contrast to the Fe phase, the cobalt compound is electrochemical inactive. Thus only the Fe phases were oxidized. The delithiated phases $Li_{1.5}Fe(SO_4)_2$ and $Li_1Fe(SO_4)_2$ can be obtained by electrochemical extraction as previously demonstrated.[17,20] However, in order to prepare them in quantity sufficient for neutron diffraction, they were obtained through chemical oxidation of $Li_2Fe(SO_4)_2$ using stoichiometric amounts of NO_2BF_4 as an oxidation agent (0.5 and 1 equivalent, respectively) in acetonitrile. These chemically delithiated samples present X-ray diffraction patterns similar to the electrochemically prepared samples.

Structural characterization

Laboratory X-ray powder diffraction (XRD) patterns were recorded with a Bruker D8 Advance diffractometer equipped with a Cu Kα radiation (λ_1 = 1.54056 Å, λ_2= 1.54439 Å) and a LynxEye detector.

Neutron powder diffraction (NPD) was performed on the high-intensity D20 diffractometer at the Institut Laue Langevin (ILL, Grenoble, France) to determine the magnetic structures of

the title compounds. NPD patterns on D20 were recorded in high-resolution conditions (take–off angle 90°) with two different wavelengths: λ = 1.544 Å and λ = 2.419 Å obtained with a Ge monochromator.

Nuclear and magnetic structures were refined using the Rietveld method as implemented in the FullProf suite of program.[21,22] For the magnetic structure determination, Bertaut's symmetry analyses[23] were carried out with the BasIReps program of FullProf suite.

Magnetic measurements

Powder samples of roughly 20-30 mg were placed into gel caps for the measurement in such a way as to avoid any motion of the sample during the measurements. Susceptibility measurements were carried out using a SQUID XL magnetometer (Quantum design), in zero field cooled (ZFC) and field cooled (FC) modes, under applied magnetic fields of 10 kOe between 350 K and 10 K. Isothermal magnetization curves M = f(H) were recorded at 2 K for each sample.

Results

Crystal structures

The crystalline quality of the four samples $Li_2Co(SO_4)_2$, $Li_2Fe(SO_4)_2$, $Li_{1.5}Fe(SO_4)_2$ and $Li_1Fe(SO_4)_2$ was checked via XRD measurements. $Li_2Co(SO_4)_2$ and $Li_2Fe(SO_4)_2$ were obtained as pure samples, while $Li_{1.5}Fe(SO_4)_2$ and $Li_1Fe(SO_4)_2$, which were prepared via chemical oxidation by NO_2BF_4, showed tiny contaminations of pristine $Li_2Fe(SO_4)_2$ and Li_2SO_4 for the former and $FeSO_4{\cdot}H_2O$ for the latter. Indeed, direct synthesis for these oxidized $Li_{1.5}Fe(SO_4)_2$ and $Li_1Fe(SO_4)_2$ phases is not possible. As a result, obtaining phase-pure compounds in a sufficient quantity to perform neutron diffraction is rather challenging. However, these contaminations were below 5%. To further check the nuclear structures, we performed Rietveld refinements of the high-resolution neutron powder diffraction (NPD) patterns recorded at 30 K for the pristine phases $Li_2Co(SO_4)_2$ and $Li_2Fe(SO_4)_2$, and at 100 K for the oxidized phases $Li_{1.5}Fe(SO_4)_2$ and $Li_1Fe(SO_4)_2$. These temperatures were chosen because they are above the Néel temperatures, as will be explained later. The NPD patterns were refined against the orthorhombic structure (space group *Pbca*) initially proposed by Isasi *et al.* for the nickel analogue $Li_2Ni(SO_4)_2$ and as previously reported by our group.[17,20,24] The results of these refinements as well as their structures are summarized in Figure SI1-2 and

Table SI1-3 (Supporting Information). The structural models derived from XRD were here fully confirmed by NPD measurements indicating that the structures were preserved between room temperature and the above-mentioned temperatures. The so far unreported Rietveld refinement of $Li_2Co(SO_4)_2$ is shown in Figure 1a with the structural data summarized in Table 1. The lattice parameters are *a* = 9.1957(3) Å, *b* = 9.0949(3) Å and *c* = 13.6783(5) Å.

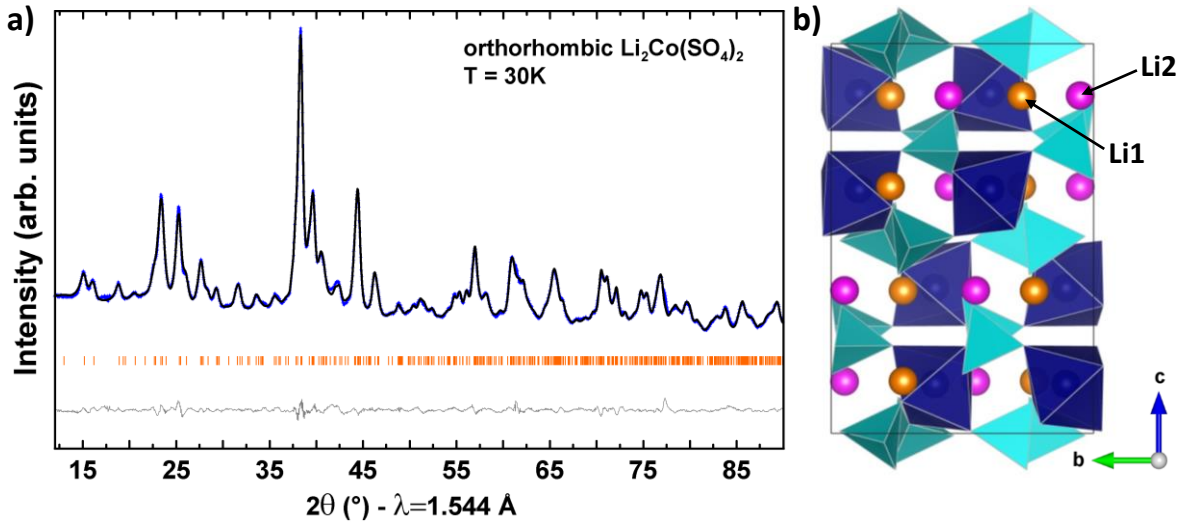

Figure 1: a) Rietveld refinement of the neutron powder pattern of orthorhombic $Li_2Co(SO_4)_2$ recorded at 30 K. The blue, black and grey lines represent the observed, calculated and difference patterns respectively. The Bragg positions are illustrated as orange bars. b) Structure of $Li_2Co(SO_4)_2$. MO_6 and SO_4 polyhedra are shown in blue and turquois, respectively. Li1 and Li2 sites are represented as orange (Li1 site) and pink spheres (Li2 site).

All atoms are located on the Wyckoff position *8c* with two distinct crystallographic Li sites and one single crystallographic site for the transition metal. Orthorhombic $Li_2M(SO_4)_2$ consists of isolated MO_6 octahedra (blue) that are connected to SO_4 tetrahedra (turquois) via their oxygen vertices (Figure 1b). The so formed 3D network hosts Li atoms (orange and pink for the Li1 and Li2 crystallographic sites, respectively) in its voids. The super-super-exchange pathways between the metal centers via two oxygen atoms (M-O-O-M) might lead to magnetic interactions as previously observed in monoclinic $Li_2M(SO_4)_2$. This was an impetus to measure the magnetic properties of the orthorhombic phases.

Magnetic properties

The temperature dependence of the molar magnetic susceptibilities of the four title compounds was probed with a SQUID magnetometer in both zero-field cooled (ZFC) and field cooled (FC) conditions. The χ=f(T) susceptibility curves present a typical Curie-Weiss antiferromagnetic behavior above 100 K, as shown in Figure 2. At lower temperatures, the susceptibility curves display a cusp indicating a long-range antiferromagnetic ordering as discussed in detail later.

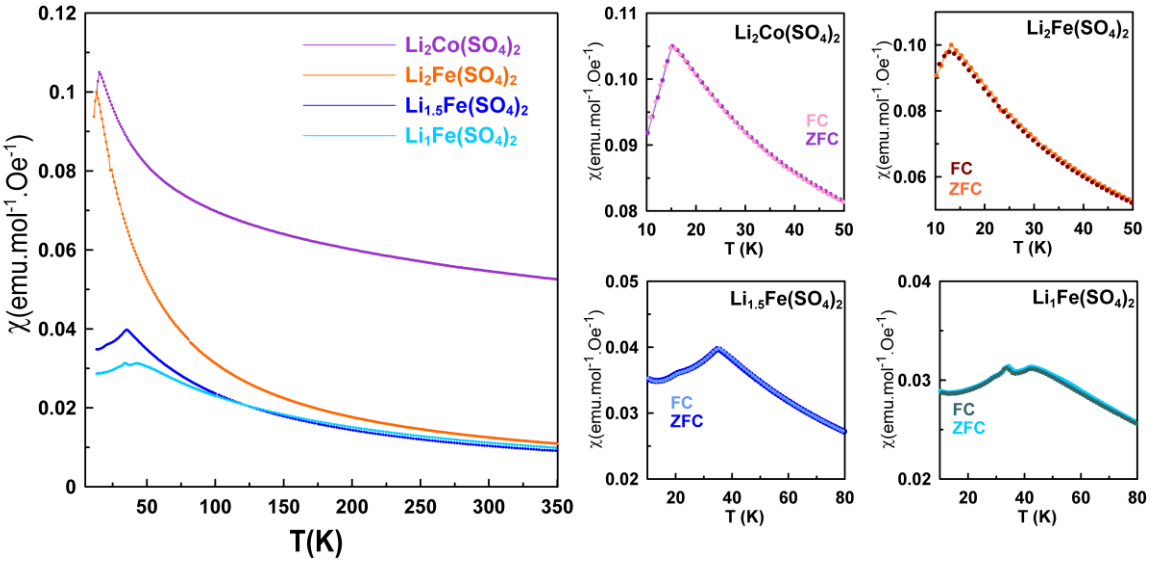

Figure 2: Temperature dependence of the molar magnetic susceptibility of orthorhombic $Li_2Co(SO_4)_2$ (purple), $Li_2Fe(SO_4)_2$ (orange), $Li_{1.5}Fe(SO_4)_2$ (blue) and $Li_1Fe(SO_4)_2$ (light blue) recorded at 10 kOe in ZFC mode. Comparison of ZFC and FC curves recorded at 10 kOe for all four compounds is shown in the right panels.

To obtain more information about the spin state of the transition metal centers and the strength of the interactions, we fitted the high temperature region (above 100 K) of the susceptibility curves to the modified Curie-Weiss equation $\chi = \chi_0 + \frac{C}{(T-\theta_{CW})}$ with χ_0 a temperature-independent component arising from the sample holder and core diamagnetism of the compound, C the Curie constant and θ_{CW} the Curie-Weiss temperature.

The final fits are shown in Figure 3. The magnetic constants (Curie-Weiss temperature θ_{CW}, frustration parameter f, Curie constant C and effective moment μ_{eff}) and the diamagnetic contributions χ_0 deduced from the fits are gathered in Table 2. The Curie-Weiss temperatures θ_{CW} show negative values pointing out an antiferromagnetic coupling between the magnetic spins of the transition metal centers. Note that θ_{CW} presents larger absolute values with increasing oxidation state of the Fe atom.

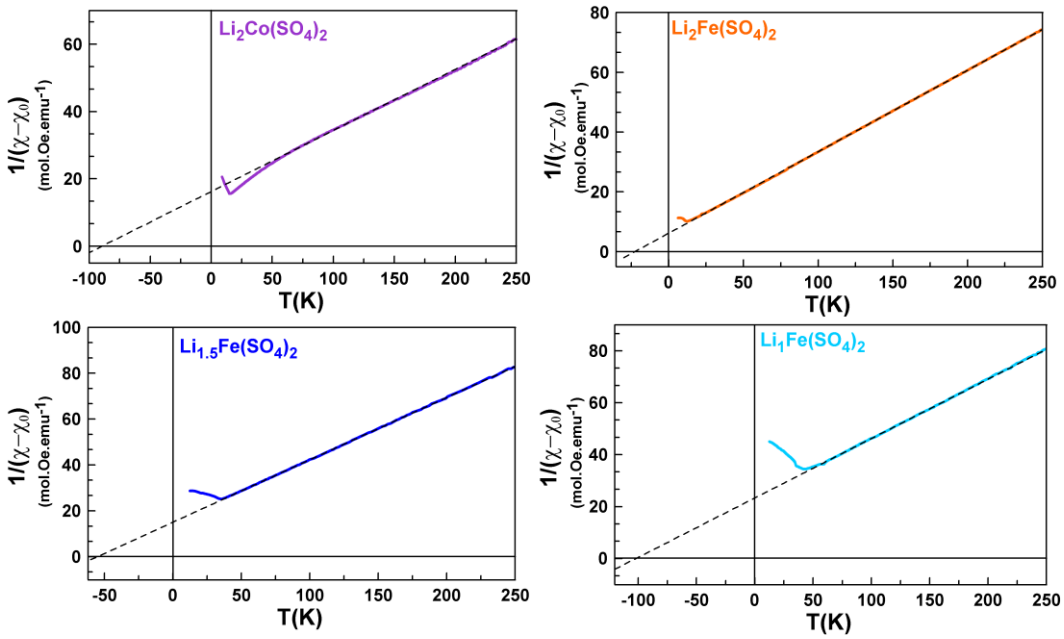

Figure 3: Inverse susceptibility fitted with the modified Curie-Weiss law for $Li_2Co(SO_4)_2$ (purple), $Li_2Fe(SO_4)_2$ (orange), $Li_{1.5}Fe(SO_4)_2$ (blue) and $Li_1Fe(SO_4)_2$ (light blue).

To calculate the effective magnetic moment μ_{eff} of a cation, various approaches can be applied. For a free ion the formula $\mu_{eff}(J) = g_J \cdot [J(J + 1)]^{1/2}$ is used with g being the Landé gyromagnetic factor and J the total angular momentum (S + L). However, due to the crystal field splitting of the d-orbitals in a coordinated cation, the effective moment is calculated either with the formula $\mu_{S+L} = [4S(S + 1) + L(L + 1)]^{1/2}$ or $\mu_S = 2 \cdot [S(S + 1)]^{1/2}$. The former is valid if the orbital angular momentum L is decoupled from the spin angular momentum S, while the latter is used for a quenched orbital moment L with a spin-only effective moment. The experimental μ_{eff} values obtained for $Li_2Fe(SO_4)_2$ and $Li_1Fe(SO_4)_2$ (5.4(1) μ_B and 5.9(3) μ_B per Fe atom, respectively) correspond well to what we expect for Fe^{2+} and Fe^{3+} in an octahedral environment with an orbital angular momentum uncoupled from the spin contribution (μ_{S+L}). For $Li_{1.5}Fe(SO_4)_2$ we obtain an effective magnetic moment of 5.4(3) μ_B. The large effective moment μ_{eff} for $Li_2Co(SO_4)_2$ (6.6(2) μ_B) can be explained by the strong spin-orbit coupling (L·S) often observed for high-spin Co^{2+} and a strong magnetic anisotropy related to the triplet ground state.[10,25,26]

Taking a closer look at the low-temperature part of the susceptibility curves (Figure 2), we can see that all four compounds show characteristic cusps of an antiferromagnetic ordering occuring at Néel temperatures of ~15 K and ~13 K for $Li_2Co(SO_4)_2$ and $Li_2Fe(SO_4)_2$, respectively. In the case of the oxidized phase $Li_1Fe(SO_4)_2$, the curve shows two cusps at ~35 K and ~42 K; the first ordering temperature (35 K) likely corresponds to the Néel temperature

of $FeSO_4 \cdot H_2O$, which was present as a minor impurity, as detected by XRD and NPD. The partially oxidized phase $Li_{1.5}Fe(SO_4)_2$ also displays two features in the susceptibility curve, at ~20 K and at ~35 K ; the latter temperature corresponds to T_N of $Li_{1.5}Fe(SO_4)_2$ as will be further demonstrated by NPD patterns, while the former one (smaller feature) remains still unknown. However, no magnetic ordering of a secondary phase was observed in the NPD patterns of $Li_{1.5}Fe(SO_4)_2$ recorded below the Néel temperature. Comparing the recorded ZFC and FC curves we can state that for $Li_2Co(SO_4)_2$ as well as for the Fe-based samples, both curves are superimposable over the whole range of temperature.

These observations prompted us to check the field dependence of the magnetization at 2 K of the orthorhombic phases $Li_2Co(SO_4)_2$ and $Li_xFe(SO_4)_2$ (x = 2, 1.5, 1) (Figure 4). The magnetization curves of the iron-based samples show a linear response as expected for a collinear antiferromagnetic ground state. $Li_2Co(SO_4)_2$ shows a magnetization curve typical for an antiferromagnet, but with a contribution likely related to a small ferromagnetic impurity in the sample that was not detected by XRD. This contribution may also be at the origin of the large χ_0 obtained for $Li_2Co(SO_4)_2$. Lastly, all the $Li_xM(SO_4)_2$ phases exhibit a rather low frustration parameter $|\theta_{CW}/T_N|$ indicating that a long range magnetic order should establish below T_N (Table 2).

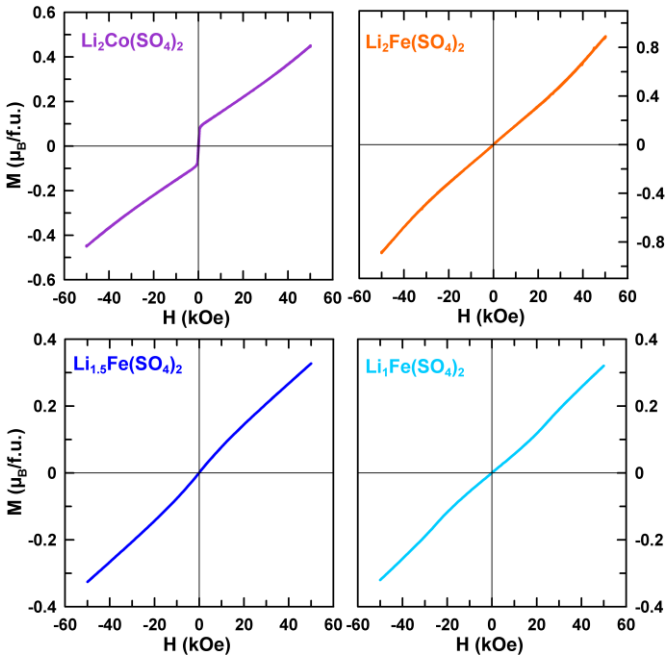

Figure 4: Isothermal magnetization curves of $Li_2Co(SO_4)_2$ (purple), $Li_2Fe(SO_4)_2$ (orange), $Li_{1.5}Fe(SO_4)_2$ (blue) and $Li_1Fe(SO_4)_2$ (light blue) recorded at 2 K.

In a next step, to gain a better understanding of the antiferromagnetic ground states of the orthorhombic phases, we conducted NPD experiments. Upon cooling the four title compounds

at the wavelength λ = 2.419 Å (Figure 5), we clearly observe a gradual growing of additional peaks assigned to the long-range antiferromagnetic ordering of the magnetic moments as illustrated in the difference pattern (green) between 30 K or 100 K (red) and 2 K (blue). At the same time, the Bragg peaks of the nuclear structure do not change suggesting that the structure remains intact over the whole temperature range. The transition temperatures observed by NPD experiments are in good agreement with the Néel temperatures deduced from SQUID measurements (Table 2).

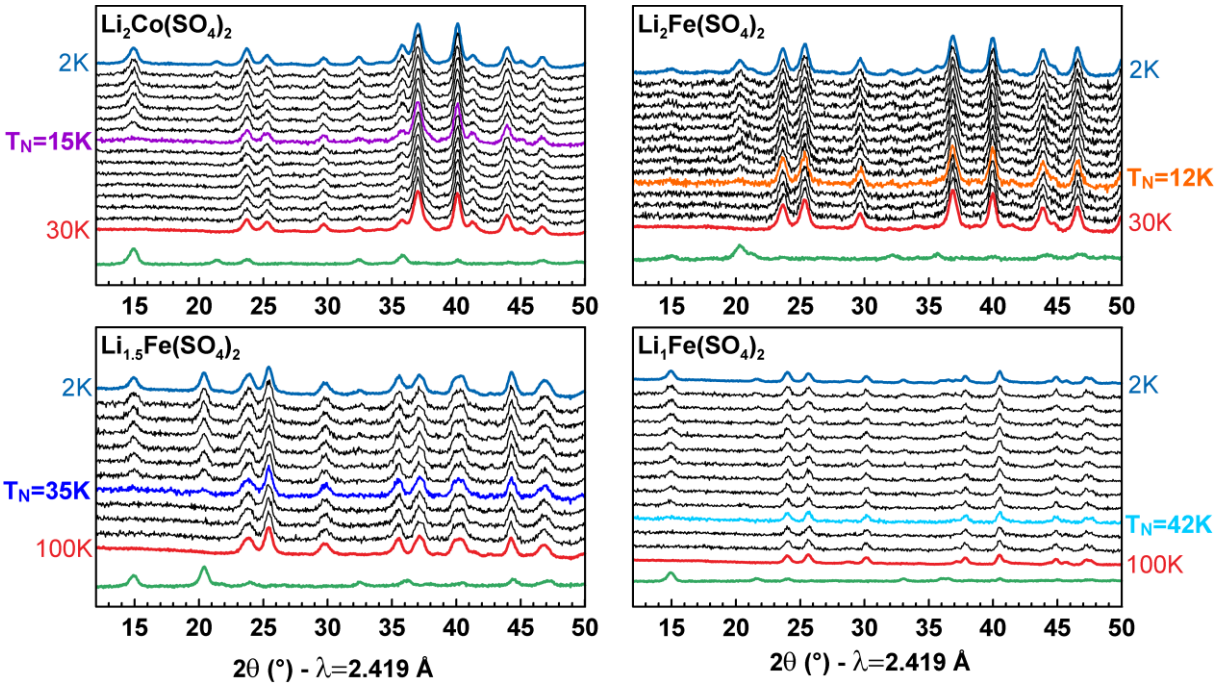

Figure 5: Evolution of the neutron powder diffraction patterns of orthorhombic $Li_2Co(SO_4)_2$, $Li_2Fe(SO_4)_2$, $Li_{1.5}Fe(SO_4)_2$ and $Li_1Fe(SO_4)_2$ while cooling the sample to 2 K. Blue patterns are measured at 2 K, while red ones are measured at 30 K for $Li_2Co(SO_4)_2$ and $Li_2Fe(SO_4)_2$ and at 100 K for $Li_{1.5}Fe(SO_4)_2$ and $Li_1Fe(SO_4)_2$. Green patterns correspond to the difference between the blue and the red patterns, i.e. solely the magnetic contribution. The patterns were recorded with a wavelength of λ = 2.419 Å. The respective Néel temperatures T_N are indicated.

Magnetic structure refinements were performed on NPD patterns recorded below the Néel temperature at 2 K with a wavelength of λ = 2.419 Å. For all compounds, all magnetic peaks can be indexed with a propagation vector **k** = (0, 0, 0), which means that the magnetic unit cell coincides with the nuclear unit cell. However, because the relative intensities of the magnetic peaks differ from one sample to another, one should expect differences in their magnetic structures. To solve the magnetic structures, we performed a symmetry analysis using Bertaut's method as implemented in the BasIReps program of the FullProf suite.[21,23] This procedure was explained in details in one of our previous papers[19] so that it is just shortly

recalled here. The 8 irreducible representations associated with the 8*c* Wyckoff site occupied by the transition metals are:

Γ_{mag} (8c) = 3 Γ_1 ⊕ 3 Γ_2 ⊕ 3 Γ_3 ⊕ 3 Γ_4 ⊕ 3 Γ_5 ⊕ 3 Γ_6 ⊕ 3 Γ_7 ⊕ 3 Γ_8

Each of these representations is composed of three basis vectors Ψ_i (i=1, 2, 3) corresponding to the moments oriented along the *a*, *b* and *c* axes. The possible spin configurations and the corresponding Shubnikov space groups are given in Table SI4. We tested all possibilities obtained by the symmetry analysis against the NPD patterns recorded at 2 K and compared the goodness of the fit for each representation. For $Li_2Co(SO_4)_2$ and $Li_1Fe(SO_4)_2$, the best fit was obtained with the irreducible representation Γ_2, with moments mainly along [001] (Ψ_3 basis vector). The refinement of the other components gives negligible values with standard deviations bigger than the refined values; so we have fixed arbitrarily to zero the *ab*-components. These two compounds therefore exhibit the exact same magnetic structure as the previously reported Ni counterpart (recalled in Figure SI4 (Supporting Information))[19] and the same Shubnikov space group *Pb'c'a'*. The Rietveld refinements (nuclear and magnetic contributions) at 2 K for $Li_2Co(SO_4)_2$ and $Li_1Fe(SO_4)_2$ are shown in Figure 6. Regarding $Li_2Fe(SO_4)_2$ the magnetic structure resolution was not so straightforward. Testing the possibilities from symmetry analysis on the 2 K pattern did not lead to any satisfactory fit. None of the eight representations could provide an accurate description of the intensities of the magnetic peaks. A moderate agreement was found with Γ_6 (Shubnikov group *Pbc'a*) with moments along *a* (Ψ_1) or Γ_8 (Shubnikov group *Pb'ca*) with moments along *b* (Ψ_2). The resulting patterns are compared to the experimental contribution (difference pattern 2 K – 30 K) in Figure SI5 (Supporting Information). Adding components along *b* and *c* (Ψ_2 and Ψ_3) for Γ_6, or along *a* and *c* (Ψ_1 and Ψ_3) for Γ_8 did not improve the quality of the fit. However, we obtain a very good agreement by mixing Γ_6 and Γ_8 representations, i.e. putting the magnetic moment as a linear combination of Ψ_1 (Γ_6) and Ψ_2 (Γ_8). The exact same situation (mixture of Ψ_1 (Γ_6) and Ψ_2 (Γ_8)) was found for $Li_{1.5}Fe(SO_4)_2$, for which we directly worked on the difference pattern 2 K – 100 K to circumvent the problem of impurities arising from the difficult preparation of that intermediate oxidized structure (Figure SI5 (Supporting Information)). The Shubnikov group corresponding to the mixing $\Gamma_6 \oplus \Gamma_8$ is $P112_1'/a$, so the set of 8 Fe atoms splits into 2 sets of four atoms, so we have two independent sites in the unit cell; however as we cannot see any structural distortion from our powder diffraction patterns, we have constrained to have the two sites the same magnitude of their magnetic moments.

The general operators of $P112_1'/a$ are 1=(x, y, z), $2_1'$ =(–x+½, –y, z+½)', -1'= (–x, –y, –z)', a=(x+½, y, –z+½) and the representative atoms of the two Fe sites are: Fe(1)≈(0.85, 0.61, 0.37) and Fe(2)≈(0.15, 0.11, 0.13). The second site representative is generated by the operator (–x, y+½, –z+½)+[1,-1, 0] of the *Pbca* space group that is no more a symmetry operator in $P112_1'/a$. The magnetic moments of the atoms in the general position generated by the above operators are: (*u*, *v*, *w*), (*u*, *v*, -*w*), (-*u*, -*v*, -*w*), (-*u*, -*v*, *w*). The constraint we have applied is that w=0 (collinear structure) for all cases and the magnetic moment of Fe(2) is opposite to the magnetic moment of Fe(1). The final Rietveld refinements of the magnetic structures of the four title compounds are gathered in Figure 6 with the respective magnetic moments summarized in Table 3.

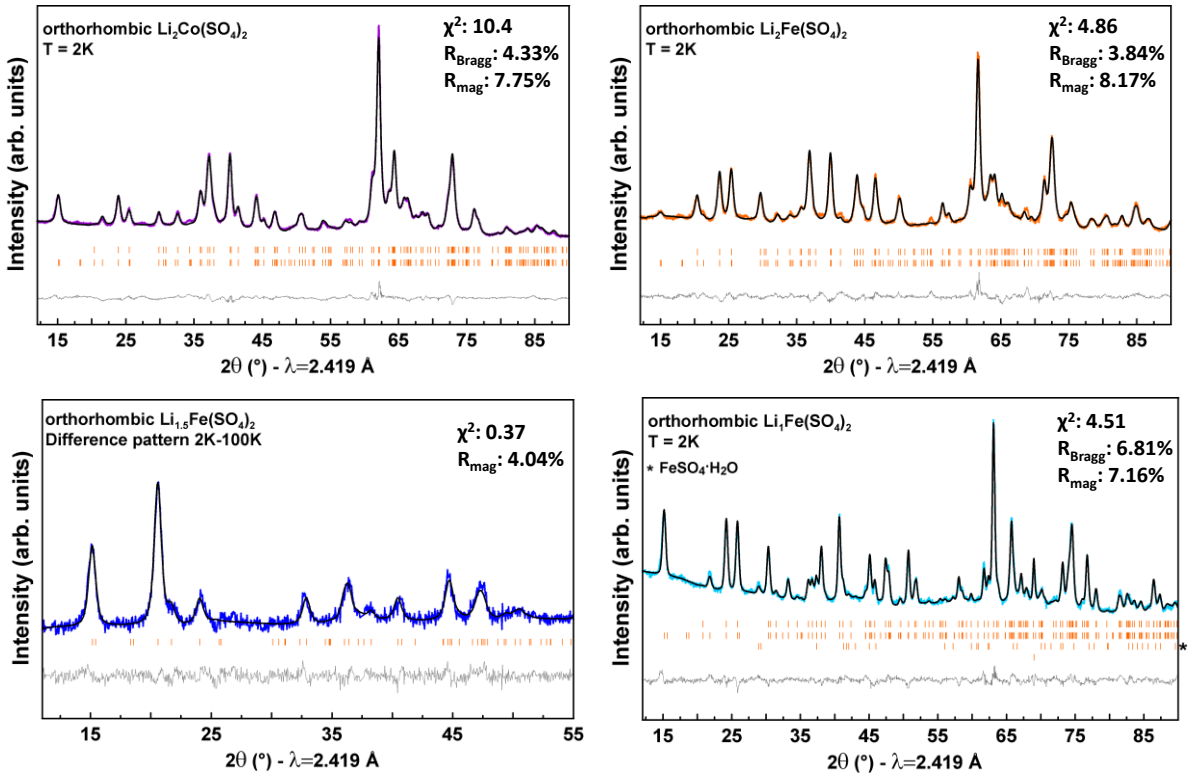

Figure 6: Rietveld refinements of the nuclear and magnetic structures of orthorhombic $Li_2Co(SO_4)_2$, $Li_2Fe(SO_4)_2$, $Li_{1.5}Fe(SO_4)_2$ and $Li_1Fe(SO_4)_2$ phases. The coloured symbols correspond to the recorded patterns. The black and grey lines represent the calculated and difference pattern, respectively. The Bragg positions are shown as orange bars, where the upper phase corresponds to the nuclear structure and the bottom one to the magnetic structure. The phase marked with a star in $Li_1Fe(SO_4)_2$ is attributed to $FeSO_4{\cdot}H_2O$. Further, the vanadium peak of the sample container was included in this refinement. For $Li_{1.5}Fe(SO_4)_2$, the refinement was done on the difference pattern 2 K – 100 K that contains only the magnetic contribution.

The magnetic structures deduced from the Rietveld refinements are shown in Figure 7. We found a long-range antiferromagnetic alignment of the magnetic spins carried by the transition metal centers of the four compounds in agreement with the results of the susceptibility measurements. For all magnetic structures - $Li_2Co(SO_4)_2$ and $Li_1Fe(SO_4)_2$ that adopt Ψ_3 (Γ_2)

as well as $Li_2Fe(SO_4)_2$ and $Li_{1.5}Fe(SO_4)_2$, for which we obtained Ψ_1 (Γ_6) and Ψ_2 (Γ_8) - the 8 magnetic moments in the cell present the sign sequence (+ + – – – – + +) where + and – signs represent the spin direction of the eight magnetic atoms taken in the same order as in the International Tables for Crystallography for position 8*c* in the *Pbca* space group. The four compounds present therefore collinear magnetic structures, which can be also described as a ferromagnetic arrangement in the [110] direction with an antiferromagnetic stacking along [001]. However, as initially guessed from the relative intensities of the magnetic reflections, the orientation of the magnetic moments differs from one compound to the other. While for $Li_2Co(SO_4)_2$ and $Li_1Fe(SO_4)_2$ the magnetic moments are found collinear to the *c*-axis, they are orientated in the *ab*-plane with zero contribution of the z-component for $Li_2Fe(SO_4)_2$ and $Li_{1.5}Fe(SO_4)_2$. Lastly, the values of the magnetic moments obtained at 2 K are in agreement with what is commonly observed: slightly lower than expected for the iron based compounds (unsaturated moments); and slightly higher for Co^{2+} as a result of the strong anisotropy.

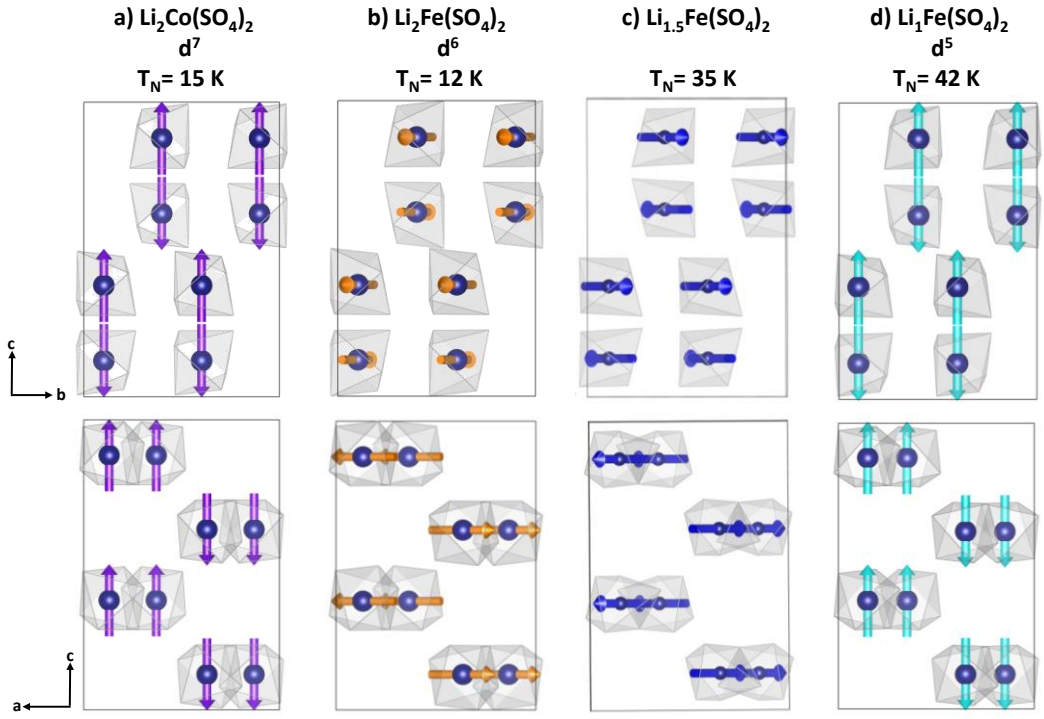

Figure 7: Magnetic structures of a) $Li_2Co(SO_4)_2$, b) $Li_2Fe(SO_4)_2$, c) $Li_{1.5}Fe(SO_4)_2$ and d) $Li_1Fe(SO_4)_2$. Magnetic moments are represented as arrows through the transition metal center shown as blue spheres. For the sake of clarity, Li, S and O atoms are omitted.

Discussion

For all four title compounds, susceptibility measurements as well as NPD experiments revealed a long-range antiferromagnetic arrangement of the magnetic spins. $Li_2Co(SO_4)_2$ and

$Li_1Fe(SO_4)_2$ are described in the Shubnikov space group *Pb'c'a'* with the sign sequence (+ + – – – – + +), i.e. the same Shubnikov space group as in the previously reported orthorhombic $Li_2Ni(SO_4)_2$ phase.[19] Regarding $Li_2Fe(SO_4)_2$ and $Li_{1.5}Fe(SO_4)_2$, the magnetic structure is found to be a mixture of representations Γ_6 and Γ_8 with the magnetic space group $P112_1'/a$ in which we have applied constraints to the magnetic moments of the two independent sites (see above). The magnetic moments have been constrained to be within the (*a*,*b*)-plane and we obtain the same spin sequence (+ + – – – – + +). First of all, we should note that having a mixture of representations is pretty uncommon and only about 10% of the magnetic structures show such a situation.[27] This case has been reported for compounds such as $RbMnF_4$ and orthoferrites.[27,28] Moreover, having a monoclinic symmetry for the magnetic space group indicates that the nuclear structure should also be of monoclinic symmetry.[29] However, in the present case, we could not identify any monoclinic distortion based on the Rietveld refinements of the XRD patterns of $Li_2Fe(SO_4)_2$ and $Li_{1.5}Fe(SO_4)_2$.[17] Indeed, the Bragg peaks present an intrinsic broadening caused by the mechano-chemical synthesis approach, and refining the structural model in a monoclinic symmetry is almost impossible as the number of parameters is increased a lot and they may be highly correlated.

The magnetic structures of $Li_xM(SO_4)_2$ show an identical spin sequence for all compounds (M=Fe with x=2, 1.5 and 1, M=Co) and correspond to the one of $Li_2Ni(SO_4)_2$. The exchange pathways between the metal centers are therefore expected to be similar to the ones deduced for $Li_2Ni(SO_4)_2$ below T_N=28 K (Figure SI6 (Supporting Information))[19], with three super-super exchange pathways (J_1 and J_3 negative, J_2 positive) to get the observed magnetic structures as ground states.

Looking at the Néel temperatures, it appears that T_N increases from 12 K to 16 K and 28 K when going from Fe^{2+} (d^6) to Co^{2+} (d^7) and Ni^{2+} (d^8), respectively. Such a trend has been similarly observed for malonate-based $Na_2M(H_2C_3O_4)_2{\cdot}2H_2O$ phases,[30] but is exactly the opposite as what was observed for $AMSO_4F$ for instance.[10,11] Therefore caution should be exercised as there is no evident trend regarding the evolution of T_N with the population of antibonding orbitals when comparing chemically different atoms. When looking at the iron series, we observe increasing ordering temperatures from orthorhombic $Li_2Fe(SO_4)_2$ (Fe^{2+}; d^6 system) to $Li_{1.5}Fe(SO_4)_2$ and $Li_1Fe(SO_4)_2$ (Fe^{3+}; d^5 system) that are in good agreement with stronger orbital interactions due to the depopulation of the t_{2g} orbitals of the transition metal upon oxidation. The influence of the oxidation state of iron on magnetism has been also observed for $LiFeSO_4F$ and monoclinic $Li_2Fe(SO_4)_2$,[11,18] with a stronger antiferromagnetic

behavior (higher T_N, larger absolute θ_{CW}) for the isotropic Fe^{3+} (d^5) ion as compared to Fe^{2+} (d^6). Further comparing the orthorhombic $Li_2M(SO_4)_2$ compounds to their monoclinic counterparts (Table SI5 (Supporting Information)), we can state that the orthorhombic phases systematically show higher T_N and larger absolute θ_{CW} values suggesting stronger antiferromagnetic interactions. This does not come as a surprise given the structural differences of the two polymorphs, where the orthorhombic phases present shorter M-M distances and a higher density enhancing the super-super-exchange interactions.

Lastly, the magnetic structures of the herein presented orthorhombic $Li_2M(SO_4)_2$ phases with the spin sequence (+ + – – – – + +) present a reverted magnetic moment (+M → –M) by the spatial inversion (x, y, z → –x, –y, –z). The *Pb*'*c*'*a*' and $P112_1'/a$ magnetic space groups involved here present a negative character for the inversion center, thus the spatial inversion is associated with time reversal. This characteristic enables the linear magneto-electric effect to be active below T_N, which means that a magnetic field can induce an electrical polarization and *vice versa*. Intense research in the mid-1960s focused on controlling the cross-coupling of magnetic and electric properties for technical applications.[31] Especially in the data storage sector the magneto-electric effect attracted a lot of attention for the development of multiferroics.[32] However, only few materials present this quality, such as Cr_2O_3 and the yttrium iron garnet (YIG).[33–35]

In the present study, we show that all the reported orthorhombic $Li_2M(SO_4)_2$ phases present the same spin sequence as orthorhombic $Li_2Ni(SO_4)_2$.[19] Therefore we can conclude that this possible magneto-electric effect is not linked to the Ni^{2+} transition metal center, but indeed more generally to the orthorhombic structural framework of these materials and the topology of the super-super-exchange interactions between transition metals inherent to this structure type. We believe that this new insight into the relation between structure and magnetic properties should help to widen the rather small family of magneto-electric compounds in the future.

Conclusion

Temperature-dependent molar susceptibility measurements as well as neutron powder diffraction measurements revealed a long-range antiferromagnetic interaction between the transition metal centers of orthorhombic $Li_2Co(SO_4)_2$, $Li_2Fe(SO_4)_2$ and its oxidized phases $Li_{1.5}Fe(SO_4)_2$ and $Li_1Fe(SO_4)_2$. For all four phases, the effective magnetic moments deduced

from the inverse susceptibility fitted with the modified Curie-Weiss correspond to the theoretical values obtained for an unquenched orbital contribution. The magnetic structures of the four title compounds were described in the Shubnikov groups *Pb*'*c*'*a*' (irreducible representation Γ_2) ($Li_2Co(SO_4)_2$ and $Li_1Fe(SO_4)_2$) and $P112_1'/a$ ($\Gamma_6 \oplus \Gamma_8$) ($Li_{1.5}Fe(SO_4)_2$ and $Li_2Fe(SO_4)_2$), all of them enabling the linear magneto-electric effect to be active below the Néel temperature. Thus, in this study, we were able to expand this unusual feature initially observed in $Li_2Ni(SO_4)_2$ to the other transition metal centers (Co^{2+}, Fe^{2+}, Fe^{3+}) and we could show that this feature is not related to the 3d metal but is inherent to the orthorhombic structure of these phases.

Acknowledgements

The authors would like to thank Thomas Hansen for his precious help in collecting powder neutron diffraction data on the diffractometer D20 at the Institut Laue Langevin (ILL, Grenoble, France). ILL is acknowledged for allocating beamtime (Proposal 5-31-2328). L. L. acknowledges the French Agence Nationale de la Recherche (ANR) via the research project « Hipolite » for her PhD grant. M. R. acknowledges the Spanish Ministerio de Economía y Competitividad (MINECO) for her post-doctoral fellowship "Ayudas Juan de la Cierva-Formación 2014", reference number FJCI-2014-19990, as well as the support of MINECO through the project reference number ENE2013-44330-R (Proyectos I + D, Retos 2013).

Supporting Information

Rietveld refinements, structural data and structures of $Li_xFe(SO_4)_2$ (x = 2, 1.5, 1); results of symmetry analysis for the *Pbca* space group; neutron difference patterns for $Li_2Fe(SO_4)_2$ and $Li_{1.5}Fe(SO_4)_2$; magnetic structure and exchange pathways for $Li_2Ni(SO_4)_2$; magnetic information of monoclinic $Li_2M(SO_4)_2$ (M = Co, Mn, Fe(II), Fe(III)); magnetic CIF files for the four title compounds (.mcif).

References

(1) Schaak, R. E.; Klimczuk, T.; Foo, M. L.; Cava, R. J. Superconductivity Phase Diagram of NaxCoO2.1.3H2O. *Nature* **2003**, *424*, 527–529.

(2) Takada, K.; Sakurai, H.; Takayama-Muromachi, E.; Izumi, F.; Dilanian, R. A.; Sasaki, T. Superconductivity in Two-Dimensional CoO2 Layers. *Nature* **2003**, *422*, 53–55.

(3) Kornev, I.; Bichurin, M.; Rivera, J.-P.; Gentil, S.; Schmid, H.; Jansen, A. G. M.; Wyder, P. Magnetoelectric Properties of LiCoPO4 and LiNiPO4. *Phys. Rev. B* **2000**, *62* (18), 12247–12253 DOI: 10.1103/PhysRevB.62.12247.

(4) Wurm, C.; Morcrette, M.; Rousse, G.; Dupont, L.; Masquelier, C. Lithium Insertion/Extraction Into/From LiMX2O7 Compositions (M = Fe, V; X = P, As) Prepared via a Solution Method. *Chemistry of Materials* **2002**, *14*, 2701–2710 DOI: 10.1021/cm020168e.

(5) Rousse, G.; Rodríguez-Carvajal, J.; Wurm, C.; Masquelier, C. Spiral Magnetic Structure in the Iron Diarsenate LiFeAs2O7: A Neutron Diffraction Study. *Phys. Rev. B* **2013**, *88* (21), 214433 DOI: 10.1103/PhysRevB.88.214433.

(6) Terasaki, I.; Abe, S.; Yasui, Y.; Okazaki, R.; Taniguchi, H. Ruthenium Oxide as a Thermoelectric Material: Unconventional Thermoelectric Properties in Li2RuO3. *J. Mater. Chem. C* **2015**, *3 (40)*, 10430-10435 DOI: 10.1039/C5TC01619C.

(7) Modic, K. A.; Smidt, T. E.; Kimchi, I.; Breznay, N. P.; Biffin, A.; Choi, S.; Johnson, R. D.; Coldea, R.; Watkins-Curry, P.; McCandless, G. T.; Chan, J. Y.; Gandara, F.; Islam, Z.; Vishwanath, A.; Shekhter, A.; McDonald, R. D.; Analytis, J. G. Realization of a Three-Dimensional Spin–anisotropic Harmonic Honeycomb Iridate. *Nature Communications* **2014**, *5*, 4203 DOI: 10.1038/ncomms5203.

(8) Rousse, G.; Tarascon, J.-M. Sulfate-Based Polyanionic Compounds for Li-Ion Batteries: Synthesis, Crystal Chemistry and Electrochemistry Aspects. *Chem. Mater.* **2014**, *26* (1), 394–406 DOI: 10.1021/cm4022358.

(9) Tao, L.; Neilson, J. R.; Melot, B. C.; McQueen, T. M.; Masquelier, C.; Rousse, G. Magnetic Structures of $LiMBO_3$ (M = Mn, Fe, Co) Lithiated Transition Metal Borates. *Inorganic Chemistry* **2013**, *52* (20), 11966–11974 DOI: 10.1021/ic401671m.

(10) Melot, B. C.; Rousse, G.; Chotard, J.-N.; Kemei, M. C.; Rodríguez-Carvajal, J.; Tarascon, J.-M. Magnetic Structure and Properties of $NaFeSO_4F$ and $NaCoSO_4F$. *Phys. Rev. B* **2012**, *85* (9), 94415 DOI: 10.1103/PhysRevB.85.094415.

(11) Melot, B. C.; Rousse, G.; Chotard, J.-N.; Ati, M.; Rodríguez-Carvajal, J.; Kemei, M. C.; Tarascon, J.-M. Magnetic Structure and Properties of the Li-Ion Battery Materials $FeSO_4F$ and $LiFeSO_4F$. *Chemistry of Materials* **2011**, *23* (11), 2922–2930 DOI: 10.1021/cm200465u.

(12) Rousse, G.; Rodriguez-Carvajal, J.; Patoux, S.; Masquelier, C. Magnetic Structures of the Triphylite LiFePO4 and of Its Delithiated Form FePO4. *Chem. Mater.* **2003**, *15* (21), 4082–4090 DOI: 10.1021/cm0300462.

(13) Rousse, G.; Rodríguez-Carvajal, J.; Wurm, C.; Masquelier, C. Magnetic Structure of Two Lithium Iron Phosphates: A- and B-$Li_3Fe_2(PO_4)_3$. *Appl. Phys. A* **2002**, *74* (1), s704–s706 DOI: 10.1007/s003390101146.

(14) Rousse, G.; Rodríguez-Carvajal, J.; Wurm, C.; Masquelier, C. A Neutron Diffraction Study of the Antiferromagnetic Diphosphate $LiFeP_2O_7$. *Solid State Sci.* **2002**, *4* (7), 973–978 DOI: 10.1016/S1293-2558(02)01347-X.

(15) Rousse, G.; Rodríguez-Carvajal, J.; Wurm, C.; Masquelier, C. Magnetic Structural Studies of the Two Polymorphs of Li3Fe2 (PO4) 3: Analysis of the Magnetic Ground State from Super-Super Exchange Interactions. *Chemistry of materials* **2001**, *13* (12), 4527–4536.

(16) Reynaud, M.; Ati, M.; Melot, B. C.; Sougrati, M. T.; Rousse, G.; Chotard, J.-N.; Tarascon, J.-M. $Li_2Fe(SO_4)_2$ as a 3.83 V Positive Electrode Material. *Electrochem. Commun.* **2012**, *21*, 77–80 DOI: 10.1016/j.elecom.2012.04.027.

(17) Lander, L.; Reynaud, M.; Rousse, G.; Sougrati, M. T.; Laberty-Robert, C.; Messinger, R. J.; Deschamps, M.; Tarascon, J.-M. Synthesis and Electrochemical Performance of

the Orthorhombic $Li_2Fe(SO_4)_2$ Polymorph for Li-Ion Batteries. *Chem. Mater.* **2014**, *26* (14), 4178–4189 DOI: 10.1021/cm5012845.

(18) Reynaud, M.; Rousse, G.; Chotard, J.-N.; Rodríguez-Carvajal, J.; Tarascon, J.-M. Marinite $Li_2M(SO_4)_2$ (M = Co, Fe, Mn) and $Li_1Fe(SO_4)_2$: Model Compounds for Super−super Exchange Magnetic Interactions. *Inorganic Chemistry* **2013**, *52*, 10456–10466 DOI: http://dx.doi.org/10.1021/ic401280e.

(19) Reynaud, M.; Rodríguez-Carvajal, J.; Chotard, J.-N.; Tarascon, J.-M.; Rousse, G. Magnetic Structure and Properties of Orthorhombic $Li_2Ni(SO_4)_2$: A Possible Magnetoelectric Material. *Phys. Rev. B* **2014**, *89* (10), 104419 DOI: 10.1103/PhysRevB.89.104419.

(20) Lander, L.; Reynaud, M.; Carrasco, J.; Katcho, N. A.; Bellin, C.; Polian, A.; Baptiste, B.; Rousse, G.; Tarascon, J.-M. Unveiling the Electrochemical Mechanisms of $Li_2Fe(SO_4)_2$ Polymorphs by Neutron Diffraction and Density Functional Theory Calculations. *Phys. Chem. Chem. Phys.* **2016**, *18* (21), 14509–14519 DOI: 10.1039/C6CP02175A.

(21) Rodríguez-Carvajal, J. *FullProf Suite*; www.ill.eu/sites/fullprof/; www.ill.eu/sites/fullprof/.

(22) Rietveld, H. M. A Profile Refinement Method for Nuclear and Magnetic Structures. *J. Appl. Crystallogr.* **1969**, *2* (2), 65–71 DOI: 10.1107/S0021889869006558.

(23) Bertaut, E. F. Magnetic Structure Analysis and Group Theory. *J. Phys. Colloques* **1971**, *32* (C1), C1-462-C1-470 DOI: 10.1051/jphyscol:19711156.

(24) Isasi, J.; Jaulmes, S.; Elfakir, A.; Quarton, M. Crystal Structure of Dilithium Nickel Disulfate, $Li_2Ni(SO_4)_2$. *Z. Krist. - New Cryst. St.* **2001**, *216* (3), 331–332.

(25) Melot, B. C.; Chotard, J.-N.; Rousse, G.; Ati, M.; Reynaud, M.; Tarascon, J.-M. Synthesis, Structure, and Magnetic Properties of the $NaCoXO_4F{\cdot}2H_2O$ Phases Where *X* = S and Se. *Inorg. Chem.* **2011**, *50* (16), 7662–7668 DOI: 10.1021/ic200700r.

(26) Borovik-Romanov, A. S.; Karasik, V. R.; Kreines, N. M. The Antiferromagnetism of Anhydrous Sulfates of Ni^{2+}, Fe^{2+}, Co^{2+} and Cu^{2+}. *J. Exptl. Theoret. Phys.* **1957**, *4* (31), 18–24.

(27) Moron, M. C.; Palacio, F.; Rodríguez-Carvajal, J. Crystal and Magnetic Structures of RbMnF4 and KMnF4 Investigated by Neutron Powder Diffraction: The Relationship between Structure and Magnetic Properties in the Mn3+ Layered Perovskites AMnF4 (A= Na, K, Rb, Cs). *Journal of Physics: Condensed Matter* **1993**, *5* (28), 4909.

(28) Izyumov, Y. A.; Naish, V. E.; Petrov, S. B. Symmetry Analysis in Neutron Diffraction Studies of Magnetic Structures: 4. Theoretical Group Analysis of Exchange Hamiltonian. *Journal of Magnetism and Magnetic Materials* **1979**, *13* (3), 275–282.

(29) Curie, P. Sur La Symétrie Dans Les Phénomènes Physiques, Symétrie D'un Champ Électrique et D'un Champ Magnétique. *Journal de physique* **1894**, *3* (1), 393–416.

(30) Rousse, G.; Radtke, G.; Klein, Y.; Ahouari, H. Long-Range Antiferromagnetic Order in Malonate-Based Compounds $Na_2M(H_2C_3O_4)_2{\cdot}2H_2O$ (M = Mn, Fe, Co, Ni). *Dalton Trans.* **2016**, *45* (6), 2536–2548 DOI: 10.1039/C5DT04527D.

(31) O'Dell, T. H. Magnetoelectrics—a New Class of Materials. *Electronics and Power* **1965**, *11* (8), 266 DOI: 10.1049/ep.1965.0199.

(32) Fiebig, M. Revival of the Magnetoelectric Effect. *Journal of Physics D: Applied Physics* **2005**, *38* (8), R123–R152 DOI: 10.1088/0022-3727/38/8/R01.

(33) Folen, V. J.; Rado, G. T.; Stalder, E. W. Anisotropy of the Magnetoelectric Effect in Cr_2O_3. *Physical Review Letters* **1961**, *6* (11), 607.

(34) Shtrikman, S.; Treves, D. Observation of the Magnetoelectric Effect in Cr_2O_3 Powders. *Phys. Rev.* **1963**, *130* (3), 986–988 DOI: 10.1103/PhysRev.130.986.

(35) Krichevtsov, B. B.; Pavlov, V. V.; Pisarev, R. V. Giant Linear Magnetoelectric Effect in Garnet Ferrite Films. *JETP Letters* **1989**, *49* (8), 535.

Table 1: Structural data from the Rietveld refinement of the neutron powder diffraction pattern of orthorhombic $Li_2Co(SO_4)_2$ recorded at 30 K.

Orthorhombic $Li_2Co(SO_4)_2$

Space group P b c a		R_{Bragg} = 2.14 %		χ^2 = 12.7		
a = 9.1957(3) Å	*b* = 9.0949(3) Å	*c* = 13.6783(5) Å		*V* = 1143.9(8) Å^3		
Atom	Wyckoff position	*x*/*a*	*y*/*b*	*z*/*c*	Occupancy	BVS
Li1	8*c*	0.475(2)	0.7259(18)	0.3660(18)	1	0.97(23)
Li2	8*c*	0.702(2)	0.551(2)	0.6331(16)	1	1.10(31)
Co	8*c*	0.8683(14)	0.6052(15)	0.3733(10)	1	2.05(33)
S1	8*c*	0.6590(5)	0.8130(4)	0.5101(3)	1	5.86(47)
S2	8*c*	0.5739(5)	0.4307(5)	0.2737(3)	1	5.81(49)
O1	8*c*	0.5017(4)	0.7983(6)	0.5239(4)	1	2.02(29)
O2	8*c*	0.7073(5)	0.9679(4)	0.4945(4)	1	1.82(24)
O3	8*c*	0.6934(7)	0.7310(6)	0.4186(3)	1	1.96(29)
O4	8*c*	0.7442(6)	0.7542(7)	0.5936(3)	1	1.86(30)
O5	8*c*	0.4788(5)	0.4993(6)	0.3488(3)	1	2.12(36)
O6	8*c*	0.5228(7)	0.4623(5)	0.1725(3)	1	2.02(29)
O7	8*c*	0.5752(6)	0.2660(4)	0.2747(5)	1	2.01(31)
O8	8*c*	0.7239(5)	0.4861(7)	0.2761(4)	1	1.98(31)

Table 2: Magnetic parameters of the orthorhombic $Li_xM(SO_4)_2$ phases deduced from magnetic measurements and neutron diffraction, and compared to the expected theoretical values.

		$Li_2Co^{II}(SO_4)_2$	$Li_2Fe^{II}(SO_4)_2$	$Li_{1.5}Fe^{II/III}(SO_4)_2$	$Li_1Fe^{III}(SO_4)_2$
Electronic configuration		$d^7 : t_{2g}^5 e_g^2$ S=3/2, L=3	$d^6 : t_{2g}^4 e_g^2$ S=2, L=2		$d^5 : t_{2g}^3 e_g^2$ S=5/2, L=0
Experimental values deduced from magnetic measurements (H = 10 kOe)					
Néel temperature T_N (K)		15(1) K	13(1) K	35(2) K	42(2) K
Curie Constant C (emu.K.mol^{-1})		5.5(2)	3.7(1)	3.7(1)	4.4(1)
Curie Weiss temperature θ_{CW} (K)		-89(2) K	-22(1) K	-55(1) K	-101(2) K
χ_0 (emu·mol^{-1}·Oe^{-1})		0.039(4)	0.001(1)	0	0
Effective moment μ_{eff}		6.6(3) μ_B	5.4(1) μ_B	5.4(2) μ_B	5.9(1) μ_B
Frustration parameter $\lvert \theta_{CW}/T_N \rvert$		5.9(4)	1.6(2)	1.6(1)	2.5(2)
Experimental values deduced from neutron diffraction					
Néel temperature T_N (K)		15(3) K	12(2) K	35(2) K	42(1) K
Magnetic moment at 2 K		3.11(5) μ_B	2.98(4) μ_B	4.82(10) μ_B	4.12(9) μ_B
Expected theoretical values					
Effective moment μ_{eff}	$\mu_{eff} = g_J \cdot (J(J+1))^{1/2}$	6.6 μ_B	6.7 μ_B	-	5.9 μ_B
	$\mu_{eff} = (4S(S+1)+L(L+1))^{1/2}$	5.2 μ_B	5.5 μ_B	-	5.9 μ_B
	$\mu_{eff} = 2 \cdot (S(S+1))^{1/2}$	3.9 μ_B	4.9 μ_B	-	5.9 μ_B
Magnetic moment $m = g \cdot S$		3 μ_B	4 μ_B	-	5 μ_B

Table 3: Lattice parameters and magnetic structures of orthorhombic $Li_xM(SO_4)_2$ deduced from Rietveld refinements of NPD pattern recorded at 2 K. Components of the magnetic moments are shown along x, y and z and the resulting magnitude of the magnetic moments (M) are given for each compound. The eight magnetic atoms in the unit cell obtained by the symmetry operators (x, y, z), (–x+½, –y, z+½), (–x, y+½, –z+½), (x+½, –y+½, –z), (–x, –y, –z), (x+½, y, –z+½), (x, –y+½, z+½) and(–x+½, y+½, z) have their magnetic moments following the sequence (+ + – – – – + +).

Orthorhombic $Li_2M(SO_4)_2$ M=Co, Fe and $Li_xFe(SO_4)_2$ with x=1.5 and x=1

Magnetic structures	**k** = (0, 0, 0)			
Compound	**$Li_2Co(SO_4)_2$**	**$Li_2Fe(SO_4)_2$**	**$Li_{1.5}Fe(SO_4)_2$**	**$Li_1Fe(SO_4)_2$**
a (Å)	9.189(2)	9.269(2)	9.181(6)	9.159(4)
b (Å)	9.087(2)	9.201(3)	9.048(3)	8.918(6)
c (Å)	13.662(1)	13.669(2)	13.581(5)	13.396(3)
Irreducible Representation	Γ_2	$\Gamma_6 \oplus \Gamma_8$	$\Gamma_6 \oplus \Gamma_8$	Γ_2
Shubnikov space group	*Pb'c'a'*	$P112_1'/a$	$P112_1'/a$	*Pb'c'a'*
M_x (μ_B)	0	+2.70(5)	+3.49(12)	0
M_y (μ_B)	0	+1.27(8)	+3.32(9)	0
M_z (μ_B)	+3.11(5)	0	0	+4.12(9)
M (μ_B)	3.11(5)	2.98(4)	4.82(10)	4.12(9)

TOC Graphics

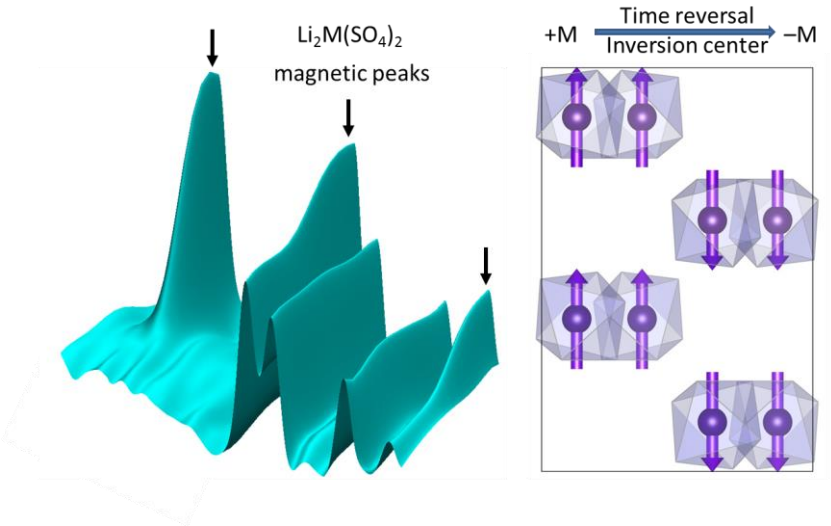

The orthorhombic $Li_2M(SO_4)_2$ phases present a long-range antiferromagnetic ordering of the magnetic moments as revealed by molar susceptibility measurements as well as neutron powder diffraction. Their magnetic structures display a possible linear magneto-electric effect owing to the association of time reversal with the inversion center.